Journal of Micromechanics and Microengineering



# MEMS cantilever based magnetic field gradient sensor

OPEN ACCESS
IOP Publishing

Made open access 14 November 2017
Journal of Micromechanics and Microengineering

J. Micromech. Microeng. **27** (2017) 055014 (8pp)

https://doi.org/10.1088/1361-6439/aa654f

# MEMS cantilever based magnetic field gradient sensor

**Alexander Dabsch**[1], **Christoph Rosenberg**[1], **Michael Stifter**[1,2] **and Franz Keplinger**[1]

[1] Institute of Sensor and Actuator Systems Vienna, Vienna University of Technology, Gusshausstraße 27-29, Austria
[2] Center for Integrated Sensor Systems, Danube University Krems, Wiener Neustadt, Viktor Kaplan Straße 2, Austria

E-mail: alexander.dabsch@tuwien.ac.at

Received 14 December 2016, revised 3 March 2017
Accepted for publication 8 March 2017
Published 5 April 2017

**Abstract**

This paper describes major contributions to a MEMS magnetic field gradient sensor. An H-shaped structure supported by four arms with two circuit paths on the surface is designed for measuring two components of the magnetic flux density and one component of the gradient. The structure is produced from silicon wafers by a dry etching process. The gold leads on the surface carry the alternating current which interacts with the magnetic field component perpendicular to the direction of the current. If the excitation frequency is near to a mechanical resonance, vibrations with an amplitude within the range of 1–$10^3$ nm are expected. Both theoretical (simulations and analytic calculations) and experimental analysis have been carried out to optimize the structures for different strength of the magnetic gradient. In the same way the impact of the coupling structure on the resonance frequency and of different operating modes to simultaneously measure two components of the flux density were tested. For measuring the local gradient of the flux density the structure was operated at the first symmetrical and the first anti-symmetrical mode. Depending on the design, flux densities of approximately 2.5 $\mu$T and gradients starting from 1 $\mu$T mm$^{-1}$ can be measured.

Keywords: cantilever, gradient sensors, magnetic field, MEMS

(Some figures may appear in colour only in the online journal)

## 1. Introduction

To measure a magnetic field gradient, normally two or more sensor elements are needed. The most common method applies two hall sensors but these elements suffer from large offsets. An alternative would be a single sensor element that is shifted mechanically requiring an exact positioning system that restricts the applicability. A possible solution are cantilever based sensor systems. Such sensors can be applied for example for magnetic resonance tomography (MRTs) or for dipole characterization (e.g. CERN Large Hadron Collider (LHC)) cryodipole [1]) where the sensor can measure local variations of the flux density. These mechanical based sensors are frequency-selective, e.g. the current over the structure has the same frequency as an eigenvalue of the vibrating structure [2]. This principle allows to avoid interferences with AC-fields of power lines, because the mechanical frequencies are far away from those of technical sources. It is inherent to the design, that both symmetric and antisymmetric modes can be excited at the same time. The individual resonance frequencies of those modes can be designed to differ substantially and do not influence each other. So it is possible to switch between these frequencies to perform different measurements, e.g. to measure the $x$- and $y$-component or a component of the gradient at the same time.

Such frequency-selective-structures operate with high quality factors $Q$, exhibiting high oscillation amplitudes and offering high signal to noise ratios for the readout [3].

One challenge is to handle the temperature dependence of the resonance frequency which causes a shift of the resonant peak. The mechanical temperature dependence of the material is described by the TCE (temperature coefficient

 

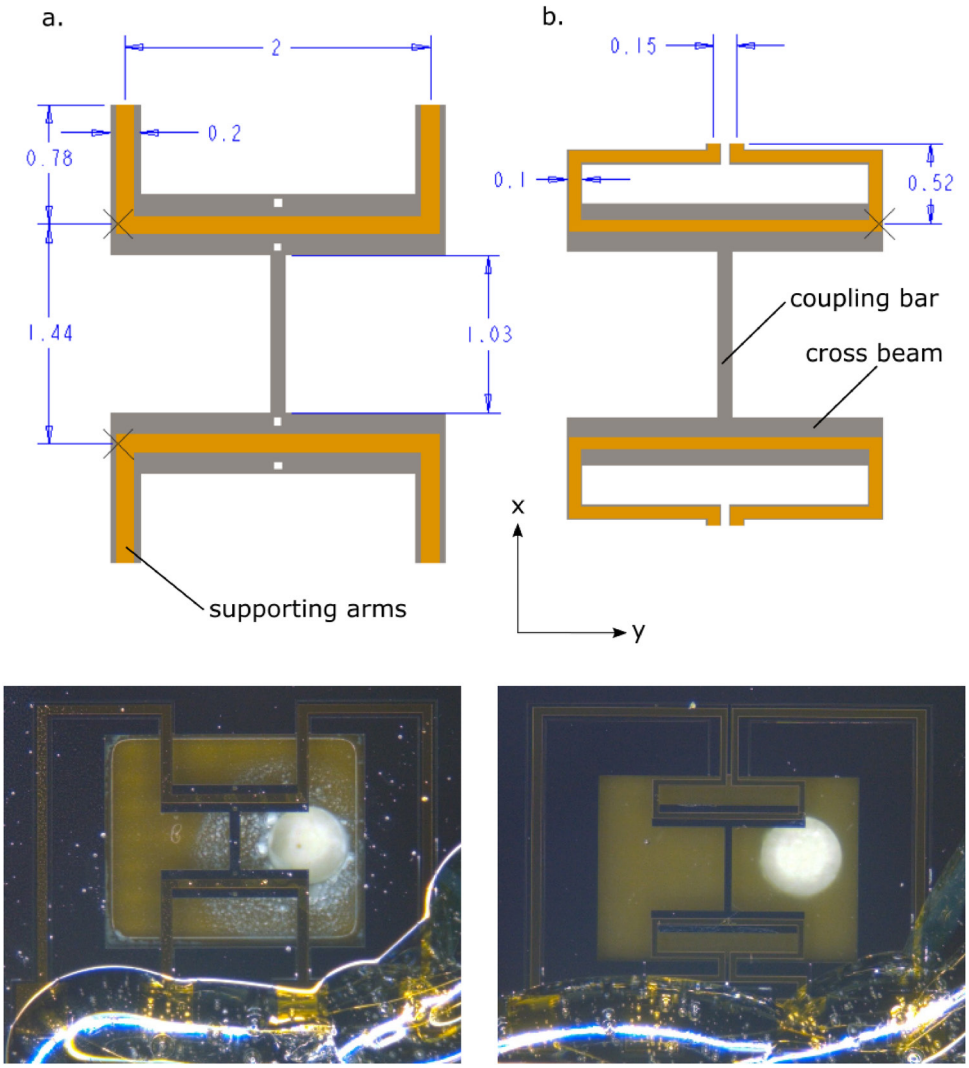


**Figure 1.** Design of the two tested structures (a) H-shaped-structure (b) Ω-structure.

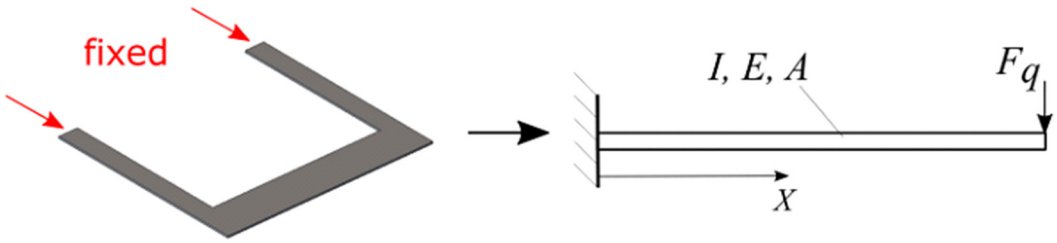


**Figure 2.** Model for a U-shaped cantilever. $F_q$ is the replacement force, $E$ is the Young's modulus of the material used, $I$ is the second moment of inertia for the specific application, and $A$ is the cross section of the cantilever.

of Young's modulus). The TCE of silicon in uniaxial-load cases is approx. $-64$ ppm °C$^{-1}$ at room temperature (25 °C) and $-75$ ppm °C$^{-1}$ at 125 °C [3].

Figure 1(a) depicts a structure that allows the measurement of two components of the flux density ($B_x$, $B_y$) and one of the gradient tensor ($\partial B_x/\partial x$). Due to the relative short supporting arms the temperature dependency of the resonant frequency is relative high. Additionally, the sensitivity for the field in the $y$-directions is much smaller than in the $x$-direction. In contrast, the structure in figure 1(b) enables the measurement of both components with similar sensitivity and with strongly reduced temperature dependency.

## 2. Design

### 2.1. Beam theory

To simplify the mathematical problem, the U-shaped structure is reduced to a simple Euler–Bernoulli-Beam with an additional mass at the ends of each single cantilever (see figure 2),

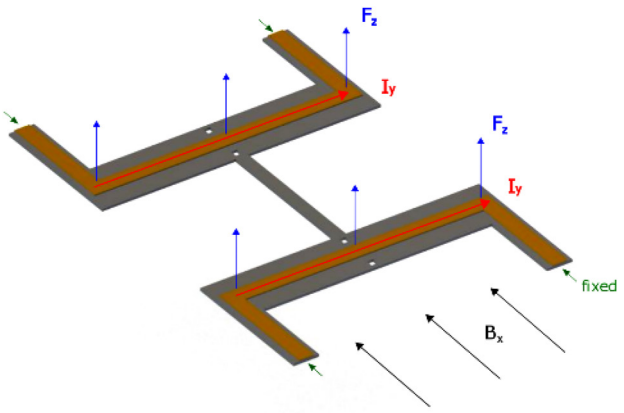


**Figure 3.** H shaped cantilever with flux density in $x$-orientation to stimulate symmetric modes.

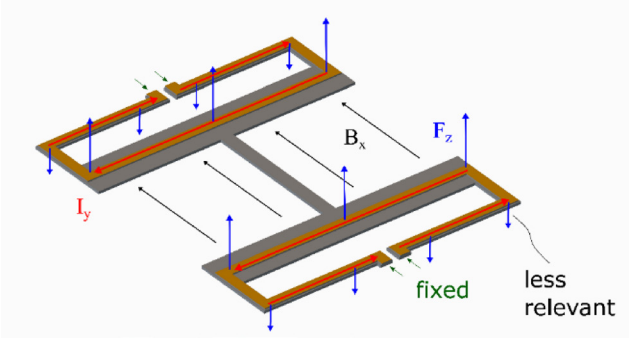


**Figure 4.** Ω Structure with flux density in $x$-orientation and the relevant forces for the symmetric modes.

where, $w$ is the displacement in $z$ direction, $\rho$ is the mass density, and $F_q$ is the distributed load.

Taking a single force instead of the coupling bar is a suitable approximation for symmetric modes.

Solving the Euler–Bernoulli differential equation with respect to the given boundary conditions delivers the characteristic polynomial for the eigenvalues for a U-shaped cantilever.

$$1 + \cos(\kappa L)\cosh(\kappa L) + \mu\kappa L(\cos(\kappa L)\sinh(\kappa L) - \sin(\kappa L)\cosh(\kappa L)) = 0 \tag{1}$$

$$\text{with } \kappa = \sqrt[4]{\omega^2 \frac{\rho A}{EI_y}} \text{ and } \mu = \frac{m}{\rho A L}. \tag{2}$$

### 2.2. Design of the structures

Measuring a gradient field requires a well-defined distance between the two points of measurement. The coupling bar between the substructures of the MEMS is necessary to couple both structures so that they can vibrate with the same frequency. This is required as the fabrication process always causes some structural differences leading to different resonance frequencies. Especially a temperature gradient can increase this mismatch and deteriorate the measurement [4].

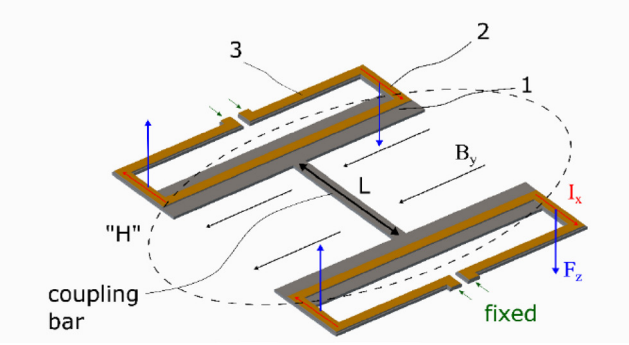


**Figure 5.** Ω structure with flux density in $y$-orientation and the relevant forces for the anti-symmetric mode.

The coupling bar between the two substructures can be represented in the model by the total energy of the coupling structure $E_{\text{tot}}$. It can be divided into two parts. The first one describes the potential energy, which is given by:

$$E_{\text{pot}}(y) = \frac{1}{2}\int_0^L \frac{M^2}{EI}\mathrm{d}z - \int_0^L pw\mathrm{d}z \tag{3}$$

$$M = -EIy^4 \tag{4}$$

Hence, the first integral is the strain energy and the second the load applied. The kinetic energy, is given by:

$$E_{\text{kin}} = \frac{\rho A}{2}\left[\int_0^L \dot{w}^2\mathrm{d}z + \int_0^L L^2\dot{\varphi}^2\right], \tag{5}$$

where the first integral describes the linear movement and the second the rotational energy. In this case $\dot{w}$ represents the linear velocity and $\dot{\varphi}$ is the angular velocity. Therefore, the interconnection for these simple structures can be modelled by the interconnection parameter:

$$K \to K[f(EI/L_{\text{i}})], \tag{6}$$

where $K$ is a function of the Young's modulus and $L_{\text{i}}$ is the length of the interconnection. $K = 0$ corresponds to two single structures with no connection and for $K = 1$ the same vibration amplitude occurs on both structures. The interconnection parameter cannot be higher than one. The most easily controllable parameter for design is the width $b$.

$$I = bh^3/12. \tag{7}$$

The Young's modulus is given by the wafer's material. The choice of the length $L$ of the coupling bar (see figure 4) determines the sensitivity of the sensor. A short connection bar is suitable for large gradient fields, while small values it has to be elongated at the cost of the spatial resolution [5].

The remaining parameter is the width of the coupling bar. The eigenfrequency of the cantilever depends first on its own and second on the eigenfrequency of the other cantilever due to the coupling bar. A too stiff coupling bar (large width) stimulates the other cantilever too much and a too thin interconnection is not able to compensate the difference between both substructures. A too small width $b$ causes a weak coupling between the both substructures due to a smaller stiffness of the coupling bar. Different resonance frequencies of the

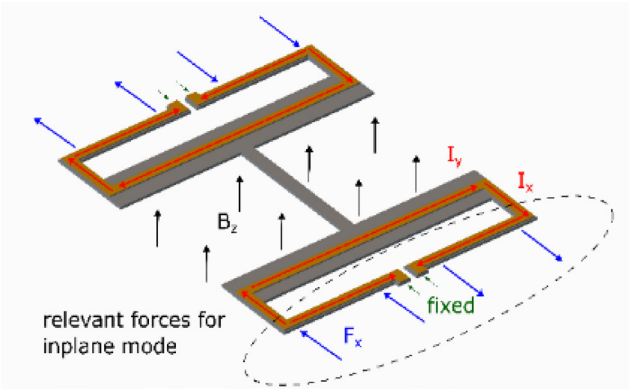


**Figure 6.** Ω structure with flux density in $z$-orientation and the relevant forces for the anti-symmetric mode.

**Table 1.** Parameters for critical current calculation.

| Symbol | Quantity | Value |
|---|---|---|
| $A_q$ | Cross section $bh$ | $2 \cdot 10^{-9}\,\mathrm{m}^2$ |
| $L$ | Length | $5 \cdot 10^{-3}\,\mathrm{m}$ |
| $\rho$ | Resistivity | $0.022\,\mu\Omega\mathrm{m}$ |
| $Z^*e$ | Specific core length | $4.2 \cdot 1.602 \cdot 10^{-19}\,\mathrm{C}$ |
| $\Delta\sigma$ | Max. mech. stress | $5 \cdot 10^{7}\,\mathrm{N\,m^{-2}}$ |
| $\Omega_a$ | Atomic value | $10.2 \cdot 10^{-6}\,\mathrm{m^3\,mol^{-1}}$ |
| $N_A$ | Avogadro constant | $6.022 \cdot 10^{23}\,\mathrm{1\,mol^{-1}}$ |

substructures due to geometrical inaccuracies cause a beat between the bars. A measurement with a test structure with half the width b revealed a too weak coupling. Two slightly different resonance peaks (3961 Hz and 3969 Hz) occur combined with high quality factor and hamper the measurement at a single frequency.

The quality factor $Q$ of the system is smaller than that of a single cantilever. Through the interconnection both resonance frequencies of the substructures merge into one mode. With a high quality factor, a minute modification of the resonance frequency causes a substantial change in amplitude (see section 4.2).

A noteworthy advantage of the structures is the possibility to sense different orientations of the flux density at the same time. Figures 3 and 4 depict the orientation of the flux density to stimulate symmetric modes at the U-shaped and in the Omega structure. In figure 5 the orientation of the flux density and the valid currents to stimulate an antisymmetric mode are depicted.

The downwards directed force in figure 4 is less relevant, because the much shorter lever arm doesn't cause a notable deflection.

The pure inplane mode was only excitable in the Ω structure (see figure 6). The necessary force and the field intensity cannot be generated in the $xy$ direction of the H-shaped structure without overlap of vibration with other modes. To avoid electromigration the maximum current with respect to the geometry of the gold circuit is restricted at approximate 2 mA for continuous operation and 50 mA for short operations. It is not possible to use higher currents due to the limited thermal

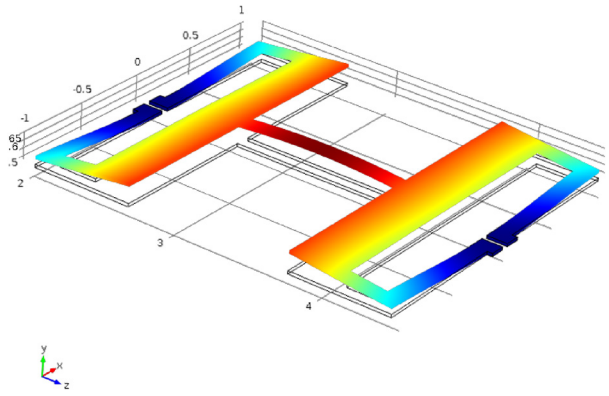

**Figure 7.** First symmetric mode at 8.156 kHz, with current in parallel direction.

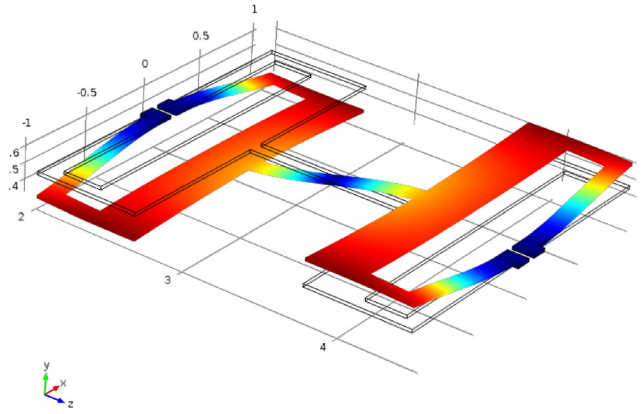

**Figure 8.** Second symmetric mode at 13.432 kHz, with current in antiparallel direction.

conductivity of the wafer under the lead [6]. The Ω structure proves an easier way to stimulate the first inplane mode (lower banding stiffness $EI_z$).

Figure 6 depicts the setup for field in $z$ direction with the relevant forces to stimulate the first inplane mode. The Lorentz forces acting on the other substructures cancel each other due to the geometry of the sensing structure.

### 2.3. Dimensioning of the Au-leads

The critical current for the leads which is mentioned in section 2.2 is calculated according to Blech *et al* [7] considering that the maximal stiffness gradient compensates gaps, generated by electro migration. This is based on occurring alternating tensile and compressive stresses. In the presented structures, tension and compressive stress occurs equally. The supply voltage has no DC-component and, therefore [8],

$$I_c = \frac{\Omega_a \Delta\sigma}{\rho Z^* e L} A_q \tag{8}$$

$$\Omega_a = \frac{\Omega}{N_A}. \tag{9}$$

Inserting the values of table 1 delivers a critical current of 2.28 mA. This represents the maximum current for a

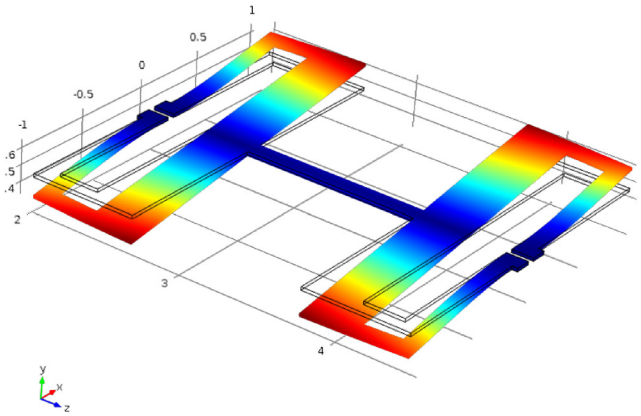

**Figure 9.** First antisymmetric mode at 11.189 kHz, with current in antiparallel direction, field configuration as shown in figure 4.

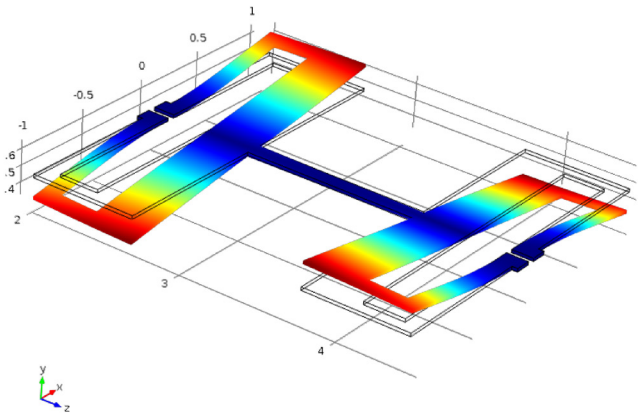

**Figure 10.** Second antisymmetric mode at 12.999 kHz, with current in parallel direction.

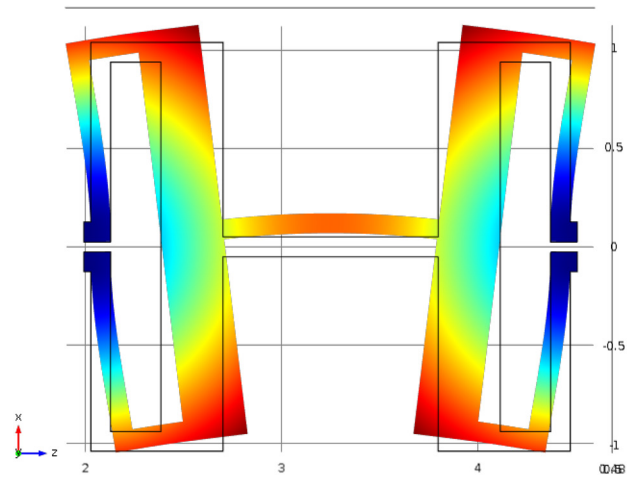

**Figure 11.** Inplane mode at 45.683 kHz, with current in parallel direction.

continuous operation to guarantee the mechanical stability of the gold circuit.

### *2.4. Material specification*

Silicon, in our case [1 0 0] oriented, exhibits an anisotropic Young's modulus with same values in $[\bar{1}\,1\,0]$ and [1 1 0] directions, but reduced values in between. For calculations and simulations, it is inevitable to know the orientation of the structure on the silicon wafers. Especially at antisymmetric modes, torsional load occurs and cannot perceived simplistically. The comparison of the simulated and measured Eigen frequencies in section 4. A. reflects the importance of the different values for each direction in space. With regard to a 3D characterization of the magnetic flux density, the different moduli are advantageous, e.g. for inplane-modes where the stiffness of the material is lower than for the other modes.

## 3. Fabrication

The MEMS structures are fabricated from a 100 mm SOI-wafer built of a 350 $\mu$m Si handle wafer, 250 nm burried oxide and a 20 $\mu$m Si device layer. The SOI wafer is coated on both sides with 70 nm low pressure chemical vapor deposition (LPCVD) silicon nitride.

Sensing structure (front side) and handle wafer (backside) are structured by a DRIE (deep reactive ion etching) process with 30 wt% KOH solution at 75 °C, the oxide layer by hydrofluoric acid. For the electrical connection the sensor is bonded with gold wires to the printed circuit board. The wires are sealed with epoxy resin (UHU® plus rapid). This is applied with a self-built dispenser.

## 4. Results

### *4.1. Simulation*

The commercial tool COMSOL Multiphysics V5.2 is used to perform the finite element method (FEM) simulation. The structures are designed in PTC® Creo Parametrics.

The elements of the stiffness matrix (see table 2) are chosen for a [1 0 0] wafer as listed in [9]. Figures 7 and 8 depict the first and second symmetric mode of an Omega structure. Comparison with figures 12 and 13 reveal the additional bending at the cross beam from the U-shaped structure.

In figures 9 and 10 the first and second asymmetric mode of the Omega shaped structure is pictured. There is no torsional stress in the cross beams but at the coupling bar.

Figures 7–13 depict the simulated symmetric and antisymmetric modes for the discussed structures. The scales in the $x$- and $z$-direction are in mm. The deflections in the $y$-orientation are in nm (stimulated with $U_{ss} = 2$ V and $B_0 = 350$ mT).

Figure 11 depicts the first simulated inplane mode for the Omega structure. This theoretical deformation is very small and due to additional flux density components in $x$- or $z$-direction combine with out-of-plane modes.

The inplane mode can be applied to measure the third field component in $y$-direction. An antiparallel current is necessary to stimulate this mode (figure 6).

In comparison to other modes the stiffness is much higher which causes a lower sensitivity due for the flux density. In our case the minimal detectable field intensity is one order of magnitude higher than for the other modes. The specific range between the resonant frequencies allows to measure three field

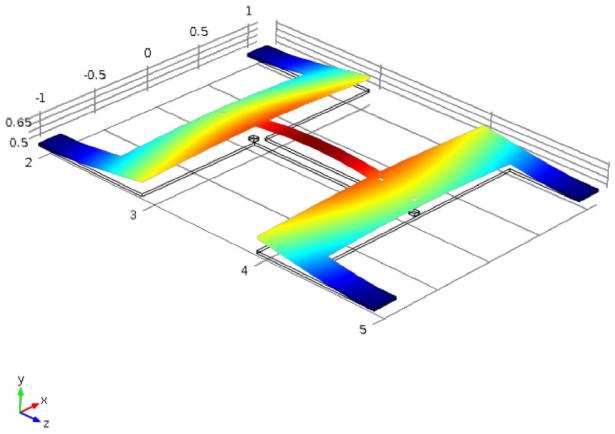

**Figure 12.** First symmetric mode of the H-shaped structure at 10.23 kHz, with current in parallel direction.

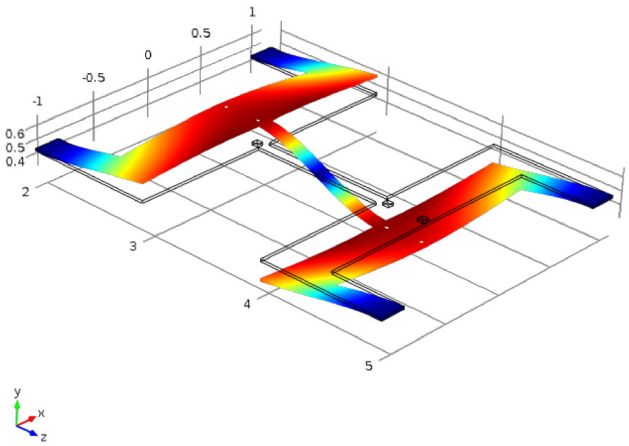

**Figure 13.** Second symmetric mode of the H-shaped structure at 22.13 kHz, with current in parallel direction.

**Table 2.** Material parameters for simulation.

| Symbol | Quantity | Value |
|---|---|---|
| $E$ | Young's modulus[a] | 170/147 GPa |
| $\nu$ | Poisson ratio[a] | 0.28/0.2 |
| $k$ | Thermal conductivity | 130 W m$^{-1}$ K$^{-1}$ |
| $\rho$ | Concentration | 2329 Kg m$^{-3}$ |
| $\boldsymbol{\alpha}$ | Thermal cofficient of expansion | $2.6 \cdot 10^6$ 1/K |
| $\mathbf{c_p}$ | Heat capacity | 700 J kg$^{-1}$ K$^{-1}$ |

[a] Depending on crystal orientation of the silicon wafer.

components at the same time. However, an inplane-displacement causes a shift of the resonant frequencies of the out-of-plane modes, because the inplane-displacement causes internal stresses.

The simulation delivers information about the stress in the coupling bar. Its value is important to match the resonance frequency of the two substructures. A further aspect is, that the coupling bar should not have a too small mass to limit the effect of the different resonance frequencies of both substructures.

Table 3 summarizes the differences between measured and simulated eigenfrequency of the sensing structure.

The etching processes, especially the wet chemical etching, cause some under etching where the 'legs' are clamped. These

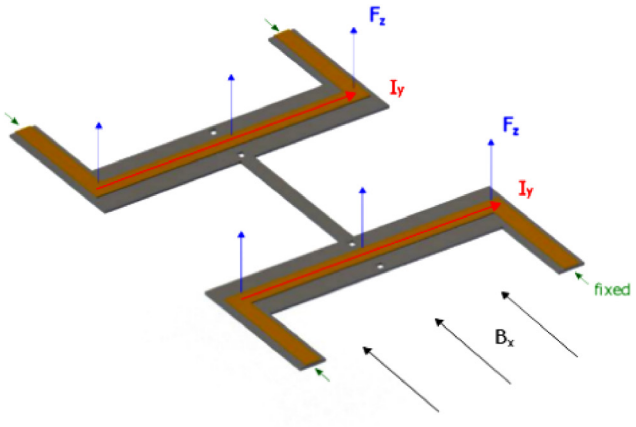


**Figure 14.** H-shaped structure: parallel current mode, with the flux density in this direction, it is used for the unequal symmetric modes.

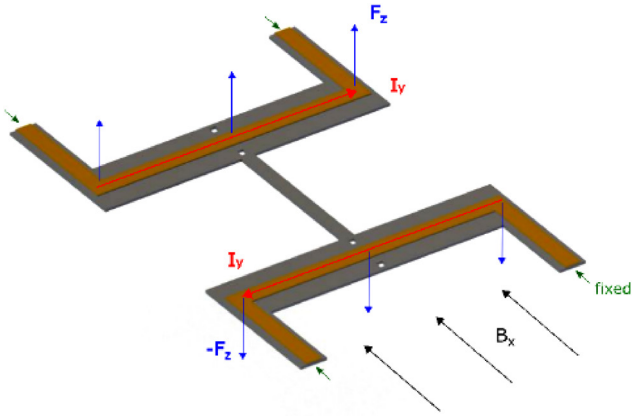


**Figure 15.** H-shaped structure: antiparallel current mode, with the flux density in this direction, it is used for the equal symmetric modes.

technological tolerances lead to small variations of the length at the legs [10]. An adjustment of the length of the supporting legs from the simulation model at the first symmetric mode, to match the resonant frequencies causes a smaller relative error at the other modes. A section of 150 nm was removed on both supporting arms. Without this adjustment, the error between simulation and measurement of the first symmetric mode of the Omega shaped structure increases to 4.18%. This reveals that the simulated model of the structure is well suited to predict the resonant frequencies.

### *4.2. Measurement*

The magnetic field is generated by two permanent magnets and the sensor is placed in between. One of these magnets can be moved by a micrometer screw. With this system, a magnetic gradient field can be generated. If the distance between the magnets and the sensor is equal on both sides, the field is homogenous. The characterization of the flux density is done with a Hall-sensor (Projekt Elektronik GmbH Berlin Teslameter FM 302) that can be arranged directly under each substructure.

The leads on the substructures are connected in series, whereas current can flow in parallel or antiparallel direction

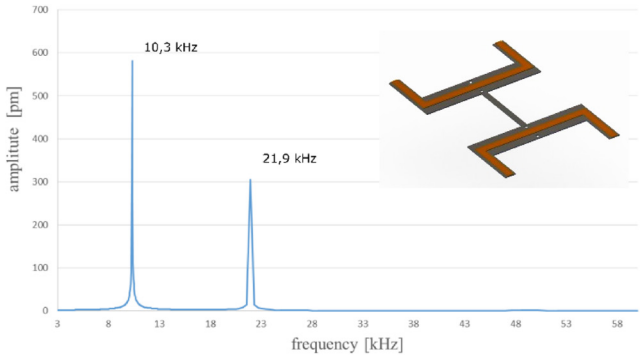


**Figure 16.** Resonance spectrum of the H-shaped structure only for symmetric excitation.

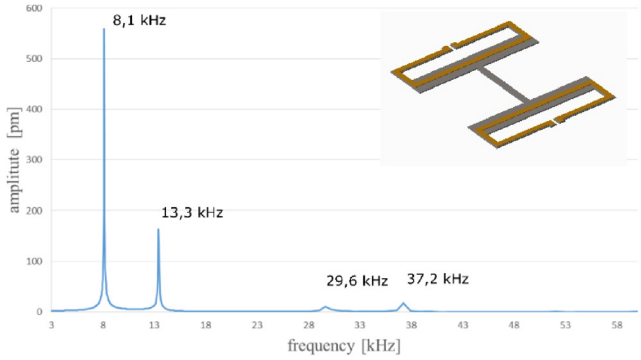


**Figure 17.** Resonance spectrum of the Ω structure only for the symmetric excitation.

to excite the first symmetric or first antisymmetric mode, respectively.

If the current direction is parallel, symmetric modes (figure 14) are excited. Every force on the cantilever is perpendicular to the flux density and the current direction as shown in figure 14. For a gradient field and symmetric excitation one of the cantilever exhibits a smaller deflection than the other one. This movement can be divided into a symmetric and an antisymmetric component (figure 15). In the first symmetric mode of the cantilever the symmetric part is much higher than the antisymmetric. For the second symmetric mode, the current is antiparallel.

To find the resonance frequencies (figures 16 and 17), a periodic chirp from 3 kHz to 60 kHz with 1000 measuring points over the complete range and additional 1000 measuring points in the vicinity of the simulated resonance frequencies is applied.

Afterwards the structure is excited with a sinusoidal current and the resulting deflections are recorded with a micro system analyzer (MSA 400 from Polytec) (see figure 18).

With the measurement of the frequency spectrum also the corresponding quality factor was determined (see table 4).

Without air damping the quality factor would increase to about $10^4$ –$10^5$ [11].

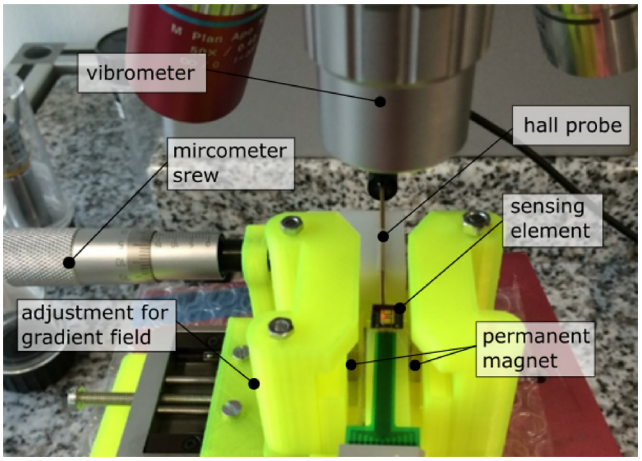


**Figure 18.** Measurement setup with the dipole and the H-shaped sensor.

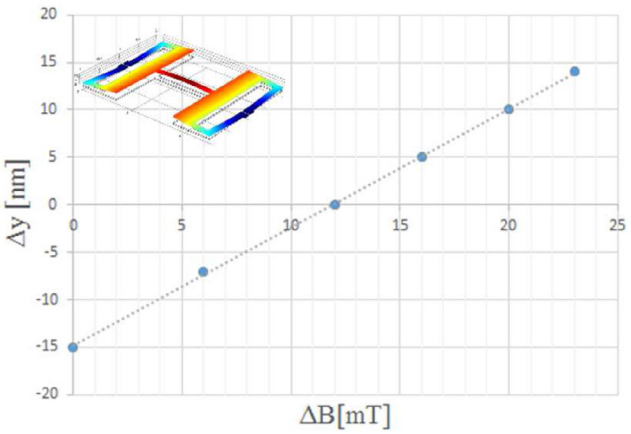


**Figure 19.** Measurement of the magnetic flux density gradient field with $B_0 = 218$ mT; excitation current 4 mA ($R = 47\ \Omega$), deflections of 526 nm at the 1st symmetric mode (8.1 kHz). $\Delta B$ represents the difference of the flux density between the two sub structures. And $\Delta y$ is the deflection difference between these two. With a SNR of 25.2 dB.

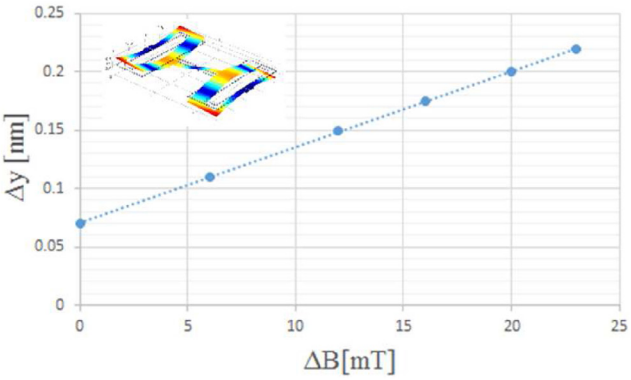


**Figure 20.** Measurement of a magnetic flux density gradient with $B_0 = 218$ mT; excitation current 4 mA ($R = 47\ \Omega$), deflections of 5.6 nm at the 4th symmetric mode (37.3 kHz). With a SNR of 24.9 dB.

**Table 3.** Resonant frequencies of the two structures and the rel. error between the simulated and the measured resonant frequencies in relation to the simulation.

| | Measured $f_{res}$ (kHz) | Simulated $f_{res}$ (kHz) | Error (%) |
|---|---|---|---|
| Ω structure | 8.13 | 8.16 | 0.37 |
| | 13.32 | 13.43 | 0.82 |
| | 29.65 | 29.89 | 0.80 |
| | 37.28 | 36.13 | 3.18 |
| H-shaped | 10.35 | 10.23 | 1.17 |
| | 21.97 | 22.13 | 0.72 |

**Table 4.** Quality factors of the respective modes of the structures in ambient conditions.

| Structure | Mode | $f_{res}$ (kHz) | Quality factor [1] |
|---|---|---|---|
| Ω structure | S1 | 8.13 | 380 |
| | S2 | 13.32 | 538 |
| | S3 | 29.65 | 932 |
| H-shaped | S1 | 10.35 | 375 |
| | S2 | 21.97 | 291 |

### *4.3. Gradient measurement*

Magnetic flux densities between 150 mT and 300 mT cause deflections of the cantilever of 300 nm–550 nm (figures 19 and 20). To keep the cantilever's vibration in a linear regime, it is common to adjust the currents like done in [1] to measure flux densities over 1 T. The flux densities in the $\mu$T regime can be measured with a ten times higher current (40–50 mA) on the structure, causing the same deflection. Without using anti-parallel current modes, it is possible to detect gradients up to 25 mT per mm at the first symmetric mode.

## 5. Conclusion and outlook

MEMS based magnetic field gradient sensors are able to measure minute differences in magnetic flux density per unit length. The presented design permits the measurement of the flux density in two directions and the gradient in one direction. This was achieved by two facing substructures coupled with a bar to ajust the resonance frequencies.

Higher accuracy will be achieved by using a vacuum chamber to eliminate air damping. Additional the measurement and control of the surface temperature to reduce the drift of the resonance frequency with the ambient temperature will further increase the accuracy of the results.

## References

[1] Stifter M 2015 MEMS $\mu$-wire magnetic field detection method@CERN *IEEE Sens. J.* **2** 15717295
[2] Kumar V 2016 Amplitude modulated Lorentz force MEMS magnetometer with picotesla sensitivity *J. Micromech. Microeng.* **26** 105021
[3] Stifter M 2012 Lorentz force actuated resonant MEMS magnetometer with capacitive read-out *Dissertation* Vienna University of Technologie
[4] Perrier T 2016 Optimization of a MEMS magnetic thin film vibrating magnetometer *IEEE Trans. Magn.* **53** 4000705
[5] Duwel A 2006 Engineering MEMS resonators with low thermoelastic damping *J. Microelectromech. Syst.* **15** 1437–45
[6] Acevedo-Mijangos J, Soler-Balcázar C, Vazquez-Leal H, Martínez-Castillo J and Herrera-May A L 2013 Design and modeling of a novel microsensor to detect magnetic fields in two orthogonal directions *Microsyst. Technol.* **19** 1897
[7] Blech I A 1976 Electromigration in thin aluminium films on titanium nitride *J. Appl. Phys.* **47** 1203
[8] Stahlmecke B 2008 Elektromigration in Gold und silber Nanostrukturen *Dissertation* Universität Duisburg-Essen p 34
[9] Hopcroft M A, Nix W D and Kenny T W 2010 What is the Young's modulus of silicon *MEMS IEEE* **19** 229–38
[10] Riesch C 2009 *Micromachined Viscosity Sensors* (Aachen: Verlag) pp 8543–2
[11] Keplinger F 2005 Contributions to miniaturized sensors *PhD Thesis* Vienna University of Technologie